Material symmetry: a key to specification of interatomic potentials

K. NALEPKA*

Department of Strength and Fatigue of Materials and Structures, Faculty of Mechanical Engineering and Robotics,
AGH University of Science and Technology, 30 Mickiewicza Ave., 30-059 Cracow, Poland

Abstract. The paper shows that symmetry forms a basis for relations between different properties of material. In this way, the key quantities for specification of an atomistic model are identified. Material symmetry distinguishes representative processes of small strains. It is proved that the errors in the densities of the energies stored in these processes determine the range of inaccuracies with which an atomistic model recreates processes of small deformations. The errors are equal to the inaccuracies in the eigenvalues of the elasticity tensor, that is in the Kelvin moduli. For cubic crystals, the elementary processes indicated by the symmetry initiate the key paths of large deformations: Bain and trigonal ones. Therefore, the substantial errors in the Kelvin moduli lead to incorrect reconstructing the metastable phases: bcc, sc and bct. The elastic constants commonly used in the literature do not provide such information as the Kelvin moduli. Using the eigenvalues of the elasticity tensor as well as other key properties indicated by the symmetry, the EAM model proposed by A.F. Voter for copper is specified. The obtained potential more accurately reproduces small and large deformations and additionally, correctly describes defect formation as well as Cu dimer properties.

Key words: crystal symmetry, interatomic potentials, elasticity, phase transformations, stacking faults.

1. Introduction

At present, more and more complex materials with wide spectra of properties are designed and manufactured, hence they find many industrial applications. One of the examples can be copper matrix composite reinforced by alumina particles. Because of the combination of high strength and electrical/thermal conductivity, the composite is used not only as electronic material but also as wear-resistant material in friction brake parts. The improvement of mechanical properties of copper by incorporating ceramic particles depends on bondings formed at phase boundaries [1]. In order to obtain interfaces with the appropriate strength, it is necessary to establish mechanical characteristics of the phase boundaries with different microstructures. These data can be derived by means of an adequate atomistic model. Such a model accurately describes interatomic interactions in the interfaces. In consequence, it enables the reconstruction of the microstructures observed in high-resolution transmission electron-microscopy (HRTEM). The characteristics of the phase boundaries derived by means of the atomistic model allow the improvement of mechanical properties but also make it possible to correctly describe the performance of the composite in the operating conditions. As a result, we can formulate criteria of limit states for the considered material.

Summing up, advanced materials presently created are not completely characterized. Models of interatomic interactions taking into account actual microstructures of the materials can provide a series of essential data [2].

The basis of presently formulated interatomic potentials are experimental and/or ab initio data. The results of the experiments are more accurate than these obtained from the first principle calculations. However, it should be underlined that the ab inito studies reveal relationships between various properties of material and identify data in areas inaccessible to the experiment. A set of data constituting the basis for a formulated model should be representative for a class of considered issues. The aim of the paper is to show that material symmetry determines data crucial for the correct description of the material behavior in the range of small and large deformations. A model which incorrectly reproduces changes induced by strain processes also inaccurately reconstructs the microstructure of the considered material. Additionally, characterization of mechanical properties obtained with the use of such a model is unreliable. Symmetry of the considered material determines eigensubspaces of the elasticity tensor. Each of them is characterized by the appropriate eigenvalue that is the Kelvin modulus [3]. If the model predicts the Kelvin moduli consistently with the experimental data, an arbitrary process of small strains is reproduced correctly. This was shown and elaborated in [4]. Because of a limited number of parameters of the model, the Kelvin moduli can differ a little from the experimental values. Then, the model reproduces small-strain processes with some acceptable inaccuracy. In the literature, the elastic constants are used instead of the Kelvin moduli. Small errors in the constants can considerably deviate one or several Kelvin moduli from the experimental values. As a result, strain processes belonging to the eigensubspace with the incorrect modulus undergo significant disturbance. This irregularity is transfered to the range of large deformations. In the paper, the Kelvin moduli are used to specify a model of interatomic interactions in copper by A.F. Voter [5, 6]. The potential has a special form which enables reproducing the process of volume deformation according to the univer-

*e-mail: knalepka@agh.edu.pl

sal binding-energy relation (UBER) [7, 8]. This relationship describes the results of the ab initio calculations and experiments. Additionally, the UBER is valid also in metal/ceramic interfaces. Therefore, this kind of potential can be applied to build a coherent model describing interfacial bonding in the frame of a Charge Transfer Ionic Potential + Embedded Atom Method approach (CTIP+EAM) [9, 10]. In the present work, parametrization conditions for the Voter model are formulated in a particularly simple form thanks to using material symmetry according to the method proposed in [4] (Sec. 2). The obtained potential, called here symmetry-based (s-b), is applied to reconstructing two key processes of large deformations: tetragonal (Bain) and trigonal ones. The derived characterizations are compared with the results provided by the original model and with the ab initio and experimental data. This reveals in what way the specification of a model with the use of data indicated by symmetry influences the description of large deformations and metastable structures (Sec. 3). The work is summarized in Sec. 4.

2. Symmetry-based specification of an interatomic potential

2.1. EAM model by Voter. The Voter model of interatomic interactions is formulated according to the Embedded Atom Method (EAM) [11]. Potentials of this kind are fast and accurate for noble metals. Therefore, they are widely applied in the literature. The EAM approach assumes that the energy of a metal crystal per atom consists of two contributions: $E_{at} = \frac{1}{2} \sum_{m=1}^{M} \phi(r_m) + F(\rho)$. The first of them comes from pair interactions of a central atom with its neighbors and the other one constitutes the energy needed to embed the central atom in electron density ρ. The density is formed by the neighboring atoms: $\rho = \sum_{m=1}^{M} f(r_m)$. Thus, the determination of the energy E_{at} requires considering certain surroundings. This area contains the atoms whose distances r_m from the central atom do not exceed a cutoff radius r_{ct}. The pair potential and the electron density are expressed as follows: $\phi(r) = D_M \left[1 - e^{-\alpha_M(r - R_M)}\right]^2 - D_M$ and $f(r) = r^6 [e^{-\beta r} + 2^9 e^{-2\beta r}]$. The form of the density function f comes from the 4s orbital, which is appropriate for copper. Both the function $f(r)$ and $\phi(r)$ have to be suppressed at the distance equal to the cutoff radius. Therefore, finally they take the form:

$$h^{sm}(r) = h(r) - h(r_{ct}) + \frac{r_{ct}}{m}\left[1 - \left(\frac{r}{r_{ct}}\right)^m\right]\left.\frac{dh}{dr}\right|_{r_{ct}}, \quad (1)$$

where $h(r) = \phi(r)$ or $f(r)$. Unlike the pair potential and the electron density, the embedding energy is not determined by an explicit formula. The function $F(\rho)$ is uniquely defined by means of an assumption. The energy F takes such a form that the process of volume deformation controlled by the lattice constant a proceeds according to the UBER:

$$F\big(a(\rho)\big) = E_{at}^{sm}(a) - \frac{1}{2} \sum_{s=1}^{S(r_{ct})} l_s \phi^{sm}\left(\sqrt{\frac{n_s}{2}} a\right). \quad (2)$$

The above formula is based on the description of the atom environment in terms of spheres of neighbors [4]. The parameters n_s and l_s characterize the face centered cubic (fcc) structure and remain constant during the strain process. The first of them constitutes the number of the sth sphere of neighbors which determines the sphere radius: $R_s = \sqrt{\frac{n_s}{2}} a$. The other parameter denotes the number of atoms belonging to this sphere. The values of the parameters are given in [4]. The cohesive energy $E_{at}(a)$ is determined by the UBER [8]: $E_{at}(\widetilde{a}) = E_{coh}(1 + \widetilde{a})e^{-\widetilde{a}}$ which is modified so as to obtain the appropriately suppressed function:

$$E_{at}^{sm}(\widetilde{a}) = E_{coh} \frac{E_{at}\big(\widetilde{a}\sqrt{1 - \epsilon}\big)/E_{coh} - \epsilon}{1 - \epsilon}. \quad (3)$$

In the above equation, the variable $\widetilde{a}$ is related to the lattice constant a in the following way: $\widetilde{a} = \eta(a - a_0)/a_0$ where $\eta = \sqrt{(9B_0\Omega_{at})/|E_{coh}|}$ while a_0, Ω_{at}, B_0 and E_{coh} constitute the equilibrium values of the lattice constant, atomic volume, bulk modulus and the cohesive energy, respectively. The parameter ϵ shifts the UBER curve in such a way that the cohesive energy equals to zero when the radius of the nearest neighbor sphere reaches the cutoff distance r_{ct}:

$$E_{at}^{sm}(\widetilde{a}_{ct}) = 0, \quad (4)$$

where $\widetilde{a}_{ct} = \eta(\sqrt{2}r_{ct} - a_0)/a_0$.

Summing up, the Voter model of interatomic interactions requires specification of five parameters: r_{ct}, β, D_M, R_M and α_M. The additional quantity ϵ is determined numerically by solving Eq. (4).

It is assumed that the potential should correctly describe mechanical properties of the crystal, formation of defects and accurately characterize the simplest structure of copper that is the dimer. This gives rise to successive conditions which specify the potential.

2.2. Elastic eigenvalues. The first two specification conditions require that the second and the third Kelvin moduli (λ_{II} and λ_{III}) are consistent with the experimental data. These relationships take particularly simple forms due to applying the symmetry relationships in the point group of the crystal [4]:

$$\frac{1}{3\Omega_{at}}\left[\frac{1}{2}\sum_{s=1}^{S} l_s(1 - 3b_s)\phi_s^{norm} + F'\sum_{s=1}^{S} l_s(1 - 3b_s)f_s^{norm}\right] = \lambda_{\text{II}}^{\exp}, \quad (5)$$

$$\frac{2}{3\Omega_{at}}\left[\frac{1}{2}\sum_{s=1}^{S} l_s b_s \phi_s^{norm} + F'\sum_{s=1}^{S} l_s b_s f_s^{norm}\right] = \lambda_{\text{III}}^{\exp}. \quad (6)$$

In the above relationships, the qualities b_s, $s = 1, ..., S$ are structural parameters like n_s and l_s while ϕ_s^{norm} and f_s^{norm} constitute normalized contributions to the Kelvin moduli from the pair interactions and the electron densities. Taking into account relationship (2), the derivative of the embedding energy F' takes the following form:

$$F' = \frac{dF}{da}\bigg|_{a_0} \frac{da}{d\rho}\bigg|_{\rho_{eq}} = -\frac{\sum\limits_{s=1}^{S}\sqrt{\frac{n_s}{2}}l_s\phi^{sm\prime}\left(\sqrt{\frac{n_s}{2}}a_0\right)}{2\sum\limits_{s=1}^{S}\sqrt{\frac{n_s}{2}}l_s f^{sm\prime}\left(\sqrt{\frac{n_s}{2}}a_0\right)},$$

where $\phi^{sm\prime} = \frac{d\phi}{dr}$ and $f^{sm\prime} = \frac{df}{dr}$. Equations (5) and (6) supplement the property of the potential according to which the volume deformation is correctly reproduced and thereby the first Kelvin modulus $\lambda_I = 3B_0$ agrees with the experimental value. Symmetry-based conditions (5) and (6) replace three Voter relationships in which the elastic constants C_{11}, C_{12} and C_{44} were taken into account. There arises a question, which of the property sets should specify the model: the moduli λ or the constants C. In order to show in what way the errors in the Kelvin moduli influence the reproducing processes of small strains, the following analysis is carried out.

An arbitrary strain process controlled by a variable ε is written in the basis of the eigenstates of the elasticity tensor $\boldsymbol{C}$ [12]:

$$\boldsymbol{\varepsilon} = \varepsilon\sum_{i=1}^{6}a_i\boldsymbol{\omega}_i, \tag{7}$$

where $a_i, i = 1, \ldots, 6$ are the coordinates of the strain versor $\boldsymbol{\varepsilon}/\varepsilon$ in the orthonormal basis $\{\boldsymbol{\omega}_i\}$. Applying the spectral decomposition of the tensor $\boldsymbol{C}$ of a cubic crystal [3, 13], the density energy stored in the arbitrary process of small strains is expressed as a linear combination of the energy densities in elementary processes [4]:

$$\Phi(\boldsymbol{\varepsilon}) = a_{\mathrm{I}}^2\Phi_{\mathrm{I}}(\varepsilon) + a_{\mathrm{II}}^2\Phi_{\mathrm{II}}(\varepsilon) + a_{\mathrm{III}}^2\Phi_{\mathrm{III}}(\varepsilon),$$
$$\Phi_i(\varepsilon) = \frac{1}{2}\lambda_i\varepsilon^2. \tag{8}$$

The elementary processes belong to different eigensubspaces of the elasticity tensor; therefore for cubic crystals $a_{\mathrm{I}}^2 = a_1^2$, $a_{\mathrm{II}}^2 = a_2^2 + a_3^2$ and $a_{\mathrm{III}}^2 = a_4^2 + a_5^2 + a_6^2$.

If the Kelvin moduli are burdened with the errors d_i: $\lambda_i = (1 + d_i)\lambda_i^{\exp}$ the energy density stored in the strain process differs from the correct one in the following way:

$$D^\Phi = \left(\Phi(\boldsymbol{\varepsilon}) - \Phi^{\exp}(\boldsymbol{\varepsilon})\right)\big/\Phi^{\exp}(\boldsymbol{\varepsilon})$$
$$= \sum_i\left(\lambda_i^{\exp}d_i a_i^2\right)\big/\sum_i\left(\lambda_i^{\exp}a_i^2\right), \quad i = \mathrm{I, II, III}. \tag{9}$$

The obtained formula uniquely identifies the error D^Φ for the arbitrary strain process which is represented by the versor $\boldsymbol{\varepsilon}/\varepsilon$ in the reference system $(a_{\mathrm{I}}, a_{\mathrm{II}}, a_{\mathrm{III}})$. The coordinates inform of the participations of the elementary processes in the considered process $\boldsymbol{\varepsilon}$. The versor $\boldsymbol{\varepsilon}/\varepsilon$ can be also oriented by two angles (θ, ϕ): $a_{\mathrm{I}} = \sin(\phi)\cos(\theta)$, $a_{\mathrm{II}} = \sin(\phi)\sin(\theta)$ and $a_{\mathrm{III}} = \cos(\phi)$ where $\theta \in\, <0, \pi/2>$ and $\phi \in\, <0, \pi/2>$. This kind of description enables us to prove that the error D^Φ takes the extremal values when the strain versor is parallel to one of the axes of the coordinate system, that is, the strain process belongs to one of the eigensubspaces of the elasticity tensor. These values are equal to the divergences d_i. Thus, the errors in the Kelvin moduli determine the accuracy with which the model reproduces small strain processes. Such

an estimation is not provided by the elastic constants. Little errors in the quantities can significantly disturb reproducing certain processes of small strains.

The energy density Φ can be expressed at the atomic level in the following way:

$$\Phi(\boldsymbol{\varepsilon}) = \frac{E_{at}(\boldsymbol{\varepsilon}) - E_{coh}}{\Omega_{at}}, \tag{10}$$

where $E_{at}(\boldsymbol{\varepsilon})$ is the energy of the deformed crystal per atom. Thus, the error D^Φ is equal to the inaccuracy with which the model predicts the change in the crystal energy due to the small strain $\boldsymbol{\varepsilon}$. As the deformation process continues, the error is transfered further into the range of large strains.

2.3. Stacking fault energy. The next datum introduced to the model is the intrinsic stacking fault energy γ_{SF}. The quantity determines the cost of the formation of the following disturbance $ABC|BCABC$ in the sequence of layers of the fcc structure. Ab initio studies show that for different metals, the energy γ_{SF} is mainly determined by the contributions from atoms belonging to four layers neighboring with the fault plane [14]. The surroundings of each of the atoms can be described by an identical set of spheres of neighbors (see Table 1). Therefore, the contributions to the stacking fault energy from the individual atoms take the same value. Both the fcc structure and the faulted one can be reconstructed by means of a periodic hexagonal cell whose base is determined by the vectors $\boldsymbol{a} = \frac{1}{2}[1\,\overline{2}\,1]a_0$ and $\boldsymbol{b} = \frac{1}{2}[1\,1\,\overline{2}]a_0$ lying in the plane (111) (see Fig. 9). Each of the cell planes parallel to the base contains three atoms. The characterization of the disturbed structure presented above enables us to express the unrelaxed stacking fault energy by means of the following formula:

$$\gamma_{SF}^{ur} = \frac{12(E_{SF}^{at} - E_{coh})}{A_h}, \tag{11}$$

where $A_h = 3\sqrt{3}a_0^2/4$ is the area of the periodic cell base while E_{SF}^{at} is the energy of an atom located in the layer neighboring with the fault plane. This energy takes the form:

$$E_{SF}^{at} = \frac{1}{2}\sum_{s=1}^{S}l_s^{SF}\phi^{sm}(\sqrt{\frac{n_s^{SF}}{2}}a_0) + F(\rho_{SF}), \tag{12}$$

where the parameters n_s^{SF} and l_s^{SF} characterize the faulted structure (Table 1) while ρ_{SF} is the electron density in which the considered atom is embedded:

$$\rho_{SF} = \sum_{s=1}^{S}l_s^{SF}f^{sm}(\sqrt{\frac{n_s^{SF}}{2}}a_0). \tag{13}$$

The embedding energy in the Voter model is not expressed explicitly. Therefore, the energy $F(\rho_{SF})$ is determined from Eq. (2) in which $a = a_{SF}$. The quantity a_{SF} constitutes the lattice constant of the fcc structure at which the electron density in a lattice site is equal to ρ_{SF}:

$$\sum_{s=1}^{S}l_s f^{sm}\left(\sqrt{\frac{n_s}{2}}a_{SF}\right) = \rho_{SF}. \tag{14}$$

s	n_s^{SF}	l_s^{SF}	l_s^{fcc}	l_s^{hcp}
1	1	12	12	12
2	2	6	6	6
3	$2\frac{2}{3}$	1	–	2
4	3	21	24	18
5	$3\frac{2}{3}$	6	–	12
6	4	9	12	6
7	5	18	24	12

Summing up, the stacking fault energy γ_{SF} is the difference of the energies of two structures: disturbed and face centered cubic ones. This difference is referred to the area of the fault plane. According to the analysis carried out above, the value of γ_{SF} is determined by the change in the energy of an atom in the fault region with respect to the cohesive energy E_{coh}. Formula (11) derived in the present work enables calculation of the unrelaxed stacking fault energy. This quantity is close to γ_{SF}. The ab initio results show that the relaxation in the direction perpendicular to the fault plane induces only insignificant decrease in the energy [15].

The intrinsic stacking fault energy is directly related to forming other defect types such as the hexagonal close packed (hcp) structure or the twin fault observed in fcc metals. The difference between the environments of atoms in the structures hcp and fcc is analogical to the change which is introduced by the intrinsic stacking fault. This change is easy to describe if we compare the system of neighbor spheres around the atom located near the fault plane with the system in the fcc structure. There can be identified two kinds of differences: additional spheres and decreases in numbers of atoms in the spheres which were present in the fcc structure. In the case of the hcp structure, both increases and decreases in numbers of atoms are twice larger (Table 1). This relation holds up to the thirteenth neighbor sphere. At that distance, the interactions between the central atom and its neighbors are negligibly small, which can be read from the UBER curves based on the ab initio calculations [8]. Accordingly, the difference of the pair interaction energies per atom in the hcp and fcc structures is twice larger than the change in the pair interaction energy induced by the stacking fault. The differences of the embedding energies remain in a similar relation. However, because of nonlinearity of the function $F(\rho)$, double increase in the electron density does not induce exactly double change in the embedding energy. Therefore, the hcp-fcc structural energy difference is related to the stacking fault energy in the following way:

$$\Delta E_{fcc \rightarrow hcp} \approx 2(E_{SF}^{at} - E_{coh}). \tag{15}$$

This relationship is confirmed by the ab initio calculations [16]. They also reveal another relation; this time between the twin energy and the stacking fault energy:

$$\gamma_T \approx \frac{1}{2}\gamma_{SF}. \tag{16}$$

Like previously, the dependence results from the relation between the changes which the twin and the stacking fault introduce into the surroundings of an atom of the fcc structure.

According to the assumption, the appropriate specification of the potential should ensure the correct prediction of the stacking fault energy:

$$\gamma_{SF}^{ur} = \gamma_{SF}^{\text{exp}}. \tag{17}$$

This quantity influences many processes of large deformations. As shown above, it determines the energies of forming different defect types observed in fcc metals, especially in grain boundaries and in heteroepitaxial structures obtained by the physical vapor deposition [17]. The stacking fault energy is introduced to the model instead of the quantity $\Delta E_{fcc \rightarrow hcp}$ used by Voter.

2.4. Vacancy formation energy. The vacancy formation energy is the next feature which is assumed for the potential specification. According to the Voter approach, the unrelaxed energy E_f^{ur} is used. It is compared with the appropriately established experimental value. The energy cost of the vacancy formation in the perfect crystal without relaxation is as follows:

$$E_f^{ur} = E_{vac} - (N-1)E_{coh}. \tag{18}$$

The quantity E_{vac} constitutes the energy of atoms located in the vacancy surroundings with the radius equal to the cutoff distance r_{ct}. Describing the atom environment by means of neighbor spheres, the following formula for the energy is derived:

$$E_{vac} = \sum_{i=1}^{I} l_i \left[\frac{1}{2} \sum_{s=1}^{S} (l_s - \delta_{is})\phi^{sm}\left(\sqrt{\frac{n_s}{2}}a_0\right) + F(\rho_i^{vac}) \right], \tag{19}$$

where the values of the structural parameters: l and n are given in Table 1 in [4], δ_{is} denotes the Kronecker delta while I is the number of the neighbor spheres contained in the vacancy surroundings. The quantity ρ_i constitutes the electron density at an atom of the sphere ith: $\rho_i = \sum_{s=1}^{S} (l_s - \delta_{is})f^{sm}\left(\sqrt{\frac{n_s}{2}}a_0\right)$. Owing to the specificity of the Voter potential, the embedding energy $F(\rho_i)$ is calculated from (2) with $a = a_i^{vac}$. Like in (14), the quantity a_i^{vac} is obtained by solving the equation:

$$\sum_{s=1}^{S} l_s f^{sm}\left(\sqrt{\frac{n_s}{2}}a_i^{vac}\right) = \rho_i^{vac}. \tag{20}$$

In order to determine the unrelaxed vacancy formation energy (18), the quantity E_{vac} is compared with the energy of the same set of atoms but in the perfect crystal; therefore $N = \sum_{i=1}^{I} l_i$.

2.5. Dimer properties. The final two parametrization conditions require that the potential correctly describes the metal dimer. According to them, the model of interatomic interactions should predict the strength E_D and the length R_D of

the dimer bond consistently with the spectroscopic data [18, 19]:

$$\phi^{sm}(R_D) + 2F(\rho(R_D)) = E_D^{\exp}, \tag{21}$$

$$-F_{at} = \phi^{sm\prime}(R_D) + 2f^{sm\prime}(R_D)$$

$$\cdot \left[E_{coh}\left(\frac{\eta}{a_0}\right)^2 (a_D - a_0)e^{-\eta\sqrt{1-\epsilon}(a_D-a_0)/a_0} \right.$$

$$\left. -\frac{1}{2}\sum_{s=1}^{S}\sqrt{\frac{n_s}{2}}l_s\phi^{sm\prime}\left(\sqrt{\frac{n_s}{2}}a_D\right) \right] \Bigg/ \tag{22}$$

$$\left[\sum_{s=1}^{S}\sqrt{\frac{n_s}{2}}l_s f^{sm\prime}\left(\sqrt{\frac{n_s}{2}}a_D\right) \right] = 0.$$

Relationship (22) constitutes the equilibrium condition. Therefore, it allows determining the dimer bond length. The obtained value should be equal to the experimental one: $R_D = R_D^{\exp}$. In (22), a_D is the lattice constant of the Cu crystal at which the electron density in a lattice site is equal to the electron density at the dimer atom:

$$\sum_{s=1}^{S} l_s f^{sm}\left(\sqrt{\frac{n_s}{2}}a_D\right) = f^{sm}(R_D). \tag{23}$$

The embedding energy in condition (21) is calculated from (2) with $a = a_D$.

Conditions (5), (6), (11), (18) derived above in which defined quantities take the experimental values can be applied to specification of an arbitrary EAM model describing interatomic interactions in fcc metals. The relationships have particularly simple forms due to using material symmetry and the description of the atom environment by neighbor spheres. Thanks to this, the proposed conditions reduce the computational cost of solving the optimization problem for the potential specification. The developed approach enables simplification of the equations to determine the embedding energies, since in the Voter model the function $F(\rho)$ is defined implicitly by means of the UBER. The above-mentioned conditions supplemented by two successive ones (21) and (22) concerning the dimer properties constitute the relationships which specify the considered potential.

3. Copper properties recreated by different EAM models

The conditions derived in the previous section are applied to the specification of the Voter potential. For this purpose, the minimization of the following function is carried out:

$$g = \sum_i \frac{(v_i - v_i^{\exp})^2}{(v_i^{\exp})^2}, \tag{24}$$

where $v_i, i = 1, \ldots, 6$ denote considered properties predicted by the model and $v_i^{\exp}$ constitute the appropriate experimental data. Optimization problem (24) is solved by the Trust-Region Method [20] implemented in Matlab package [21]. The minimization is performed with different initial points which form a representative set in the five dimensional space. As a result, the following parameters for the Voter model are obtained: $r_{ct} = 4.9456$ Å, $\beta = 4.1067$ Å^{-1}, $D_M = 0.5312$ eV, $R_M = 2.3834$ Å and $\alpha_M = 1.8816$ Å^{-1}. Additionally, the shift parameter ϵ amounts to 0.0497384 eV.

The EAM functions for the model specified with the use of the material symmetry are shown in Fig. 1. The description of small-strain processes provided by the s-b potential is presented in Table 2. The equilibrium state is such as the experimentally identified one [22–25] while the Kelvin moduli differ from the experimental values [26, 27] in the range of 3%. Therefore, the proposed model reproduces an arbitrary process of small strains in good agreement with the experiment. The distribution of errors in energy densities $D^\Phi(\varepsilon)$ is presented in Fig. 2. The arbitrary strain process $\varepsilon(\varepsilon)$ is represented by the contributions a_{II} and a_{III}. The participation of the first elementary process a_I is obtained from the relationship: $a_I^2 + a_{II}^2 + a_{III}^2 = 1$. The distribution $D^\Phi(\varepsilon)$ shows with what errors the key processes of large strains are initiated: the Bain and the trigonal paths. The first of them begins in the second eigensubspace and the other in the third subspace. Therefore, the errors D^Φ are such as for λ_{II} and λ_{III} that is 2.5% and -2.6%, respectively. The different description of small-strain processes is provided by the original Voter potential. The model correctly identifies the equilibrium state as well as the first and the third Kelvin moduli but the second modulus deviates from the experimental value by over 9%.
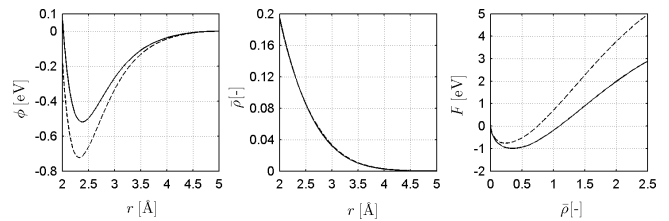

Fig. 1. EAM functions for the s-b (solid line) and Voter (dashed line) models: pair potential ϕ, electron density referred to the density at an atom of copper crystal in the equilibrium $\overline{\rho}$ and embedding energy F

Table 2
Descriptions of small-strain processes provided by the EAM models in comparison with the experimental characterization: cohesive energy (E_{coh} in eV), lattice constant (a_0 in Å), press (p in MPa), Kelvin moduli (λ in GPa) and elastic constants (C in GPa). The experimental data at the temperature 0K are given in the left column and at the room temperature in the right column

	s-b	Voter	Exp.		Mishin
E_{coh}	-3.48	-3.54	-3.48^a	-3.54^b	-3.54
a_0	3.603	3.615	3.603^c	3.615^d	3.615
p	10^{-6}	10^{-5}	0		9.0
λ_I	426.0	426.0	426.0^e	414.9^f	414.9
λ_{II}	52.6	56.1	51.3^e	47.5^f	47.3
λ_{III}	159.4	162.0	163.6^e	151.6^f	152.4
C_{11}	177.1	179.4	176.2^e	170.0^f	169.9
C_{12}	124.5	123.3	124.9^e	122.5^f	122.6
C_{44}	79.7	81.0	81.8^e	75.8^f	76.2

[a] Ref. [22], [b] Ref. [23], [c] Ref. [24],
[d] Ref. [25], [e] Ref. [26], [f] Ref. [27].

As a result, the potential improperly reproduces the processes which in a large part proceed in the second eigensubspace (see Fig. 3). Therefore, the process initiating the Bain path is burdened with 9.4% error. The trigonal path begins with the error -1%.
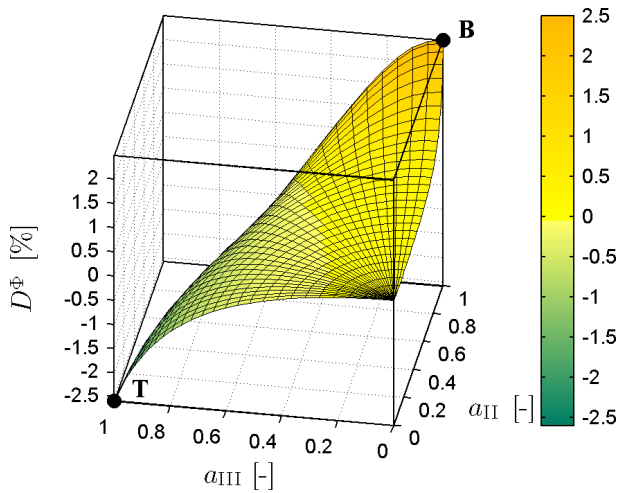

Fig. 2. Error (D^Φ) with which the s-b potential determines elastic energy density as a function of participations of the elementary processes (a_{II} and a_{III}) in a small-strain process. The errors for the processes initiating the Bain and the trigonal paths are marked by the black points $\mathbf{B}(1, 0, 2.5\%)$ and $\mathbf{T}(0, 1, -2.6\%)$, respectively
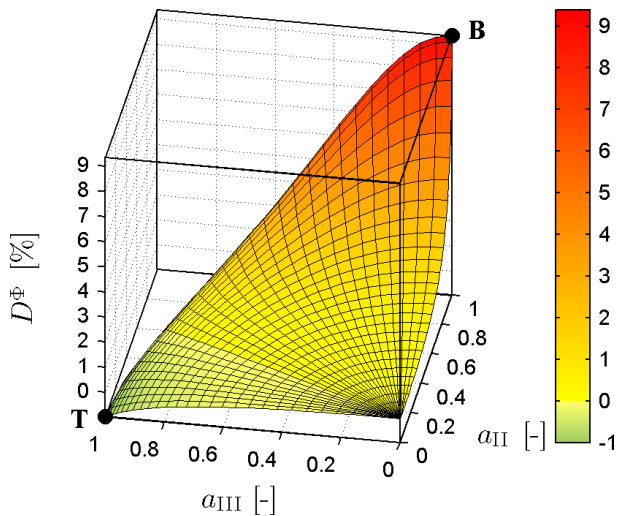
Fig. 3. Distribution of errors D^Φ for the Voter potential. The errors for the processes initiating the trigonal and the Bain paths are marked by the black points $\mathbf{B}(1, 0, 9.4\%)$ and $\mathbf{T}(0, 1, -1\%)$, respectively

Additionally, it is shown in what way the considered models reconstruct a process of uniaxial tension. The load is applied in an arbitrary direction relative to the cubic system of copper. The errors with which the s-b and Voter models predict the density of the elastic energy stored in the analyzed process are presented in a form of a surface in Fig. 4. The error function D^Φ takes the extreme values at the tension along one of cubic cell edges and when the load is applied perpendicularly to one of the octahedral planes. In the first case, the elastic energy is stored mainly in the second eigensubspace

while in the other one in the third eigensubspace. Therefore, the errors remain close to the errors in the respective Kelvin moduli.
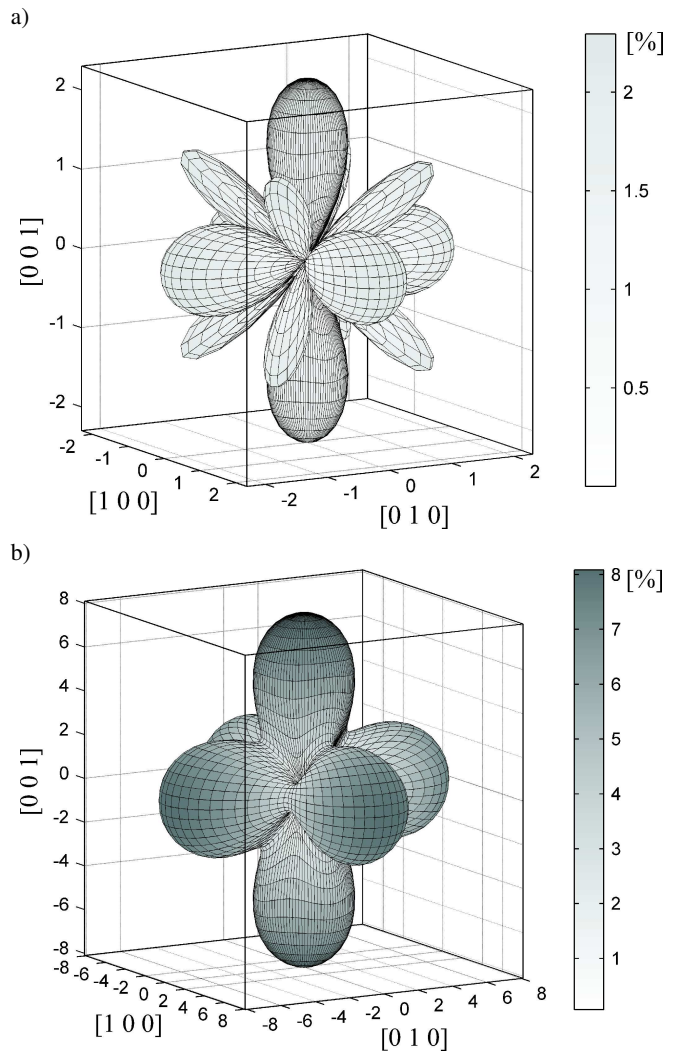
a)

b)

Fig. 4. Surface of absolute value of error in density of elastic energy stored during uniaxial tension in arbitrary direction: a) s-b model, b) Voter model

The considered potentials are compared with the Mishin et al. model [28]. It is one of more frequently used potentials for copper. The model contains 23 parameters which were specified by means of the ab initio data. The potential reproduces small-strain processes in accordance with the experiment. Although, the equilibrium structure identified experimentally is predicted at the pressure 9 MPa (see Table 2).

The characteristics of the planar defects provided by the s-b model are shown in Table 3. They are compared with the results obtained by means of the Voter and Mishin et al. potentials as well as with the experimental data [29–33]. The planar defects remain related to the hcp-fcc structural energy difference $\Delta E_{fcc \rightarrow hcp}$. Therefore, the quantity also is captured in Table 3. The proposed model predicts the energy $\Delta E_{fcc \rightarrow hcp}$ consistently with the experimental datum. The obtained value determines the magnitudes of the stacking fault and twin

energies according to the relations (15), (11) and (16). The Voter potential provides comparable results. On the contrary, the Mishin et al. model predicts higher values. It results from the specification which is based on the ab initio data.

Table 3
Energies (γ in mJ/m^2) of planar defects and structural energy difference ($\Delta E_{fcc \to hcp}$ in meV) predicted by the EAM potentials in comparison with the experimental data; s: surface with the orientation (111), SF: intrinsic stacking fault (ur: unrelaxed), T: twin

	s-b	Voter	Exp.	Mishin
$\gamma_s(111)$	1264	1232	1790[a]	1239
γ_{SF}^{ur}	36.2	36.8	–	
γ_{SF}	35.7	36.2	41.0[b], 35–45[c]	44.4
γ_T	17.9	18.2	24[d]	22.2
$\Delta E_{fcc \to hcp}$	6.3	6.5	6.2[e]	7.6

[a] For orientation Ref. [29], [b] Ref. [30], [c] Ref. [31], [d] Ref. [32], [e] Ref. [33].

The description of the vacancy formation and the characterization of the dimer bond obtained with the use of the s-b model as well as by the Voter and Mishin et al. potentials are compared with the experimental results [18, 19, 34–37] in Table 4 and Table 5, respectively.

Table 4
Energy (E_f) and volume (Ω_f) of vacancy formation predicted by the s-b model in comparison with the experimental data and the results obtained by the Voter and Mishin et al. potentials

	s-b	Voter	Exp.	Mishin
E_f [eV]	1.291	1.258	1.19[a], 1.28[b], 1.29[c]	1.272
Ω_f/Ω_{at}	0.734	0.743	0.75[d]	0.701

[a] Ref. [34], [b] Ref. [35], [c] Ref. [36], [d] Ref. [37].

Table 5
Strength (E_D in eV) and length (R_D in Å) of the Cu dimer bond obtained by the EAM potentials in comparison with the experimental data

	s-b	Voter	Exp.	Mishin
E_D	-2.056	-2.070	-2.08 ± 0.02^{a}, -2.05^{b}	-1.93
R_D	2.219	2.231	2.2197[b]	2.18

[a] Ref. [18], [b] Ref. [19].

A model which accurately reconstructs microstructure and correctly predicts mechanical properties of copper in complex materials should properly describe large deformations including the formation of metastable phases. Volume expansion is one of the key processes of large strains. Realizing it by means of a considered potential, we obtain the simplest description of the loss of continuity in material. The proposed potential reproduces the process of the volume deformation in accordance with the ab initio data [28] (see Fig. 5). A similar agreement is obtained in the case of the Voter and Mishin et al. models.

The next essential process of large deformations is the Bain path. During the process, the base of the cubic cell is uniformly extended while, in the perpendicular direction contraction occurs. As a result, a tetragonal cell with the height c and the base edge a arises. When $c/a = 1/\sqrt{2}$ the fcc structure turns into the body centered (bcc) one (see Fig. 6). In

the classical approach, the volume per atom is kept constant: $\Omega_{at} = a_0^3/4$ [38]. Therefore, the process is described by the following Green-Lagrange strain tensor:

$$\boldsymbol{E}_B(e) = e \begin{pmatrix} 1 & 0 & 0 \\ 0 & 1 & 0 \\ 0 & 0 & -2\dfrac{e+1}{(2e+1)^2} \end{pmatrix}, \quad (25)$$

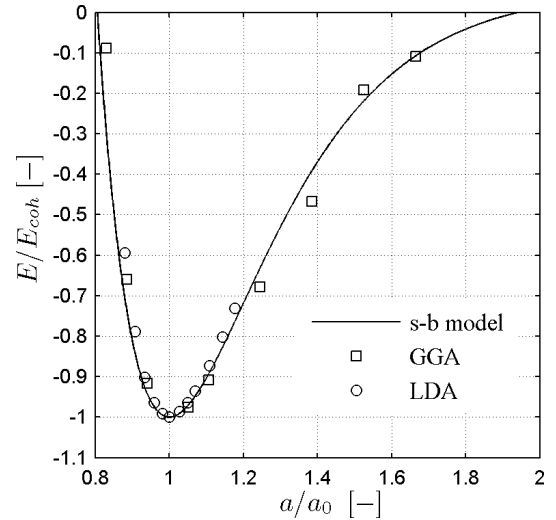where the variable e is related to the ratio $c/a = p$: $e = 0.5(1-p^2)/(p^2+2)$.

Fig. 5. Dependence of relative crystal energy per atom E/E_{coh} on relative lattice constant a/a_0 in the volume deformation process. For comparison the ab initio data are included [28]
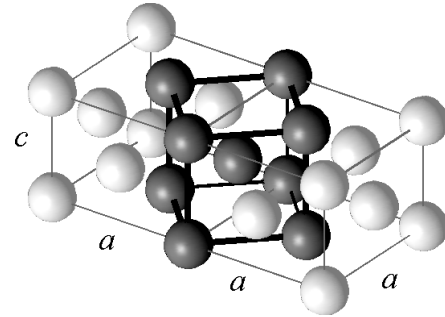

Fig. 6. Bcc structure (marked by thick solid lines) obtained at $c/a = 1/\sqrt{2}$ along the Bain path

Along the Bain path, the volume of the tetragonal cell can be allowed to relax. In this way, the actual energy difference between the structures fcc and bcc $\Delta E_{fcc \to bcc}$ is obtained. In the present work, it is noted that the classical Bain path can be replaced by a simpler linear process which also connects the fcc structure to the bcc one. For this purpose, the elements of the tensor $\boldsymbol{E}_B$ are approximated by the first-order Taylor series:

$$\boldsymbol{E}_{B.L}(e) = e \begin{pmatrix} 1 & 0 & 0 \\ 0 & 1 & 0 \\ 0 & 0 & -2 \end{pmatrix}. \quad (26)$$

The introduced process proceeds consistently with the classical Bain path in the range of small strains. Additionally, $E_{B.L}(e)$ belongs to the second eigensubspace of the tensor C. This gives rise to the conclusion that a model reproduces the beginning of the Bain path with the same accuracy as it predicts the second Kelvin modulus λ_{II}. If the error is large the path undergoes a strong disturbance, which results in an incorrect energy difference $\Delta E_{fcc \to bcc}$.

The changes in the crystal energy per atom predicted by the s-b potential along the three mentioned Bain paths as well as the changes for different tetragonal deformations are presented in Fig. 7. The results are compared with the ones obtained by means of the Voter and Mishin et al. models as well as with the experimental/ ab initio data [33, 39, 40] (see Fig. 8). Additionally, the characterizations of arising metastable structures provided by the EAM models are collated in Table 6.
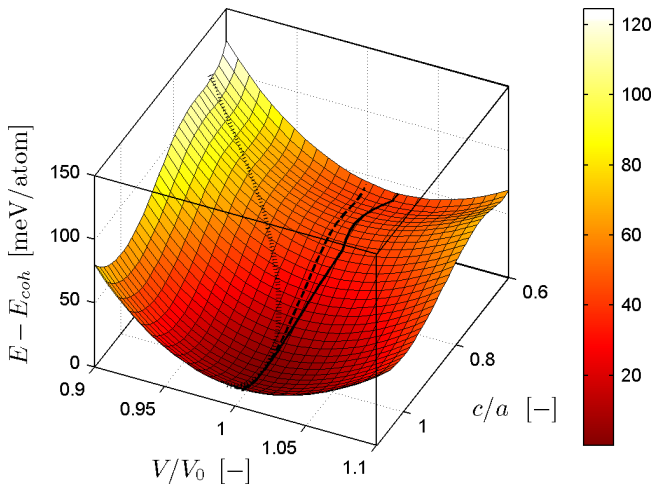

Fig. 7. Crystal energy changes ($E - E_{coh}$) predicted by the s-b model as a result of tetragonal deformations determined by ratio of the cell edges (c/a) and volume per atom referred to the equilibrium value (V/V_0). Three Bain processes are identified by thick lines: volume-relaxed (solid), volume-fixed (dashed) and linear (dotted)
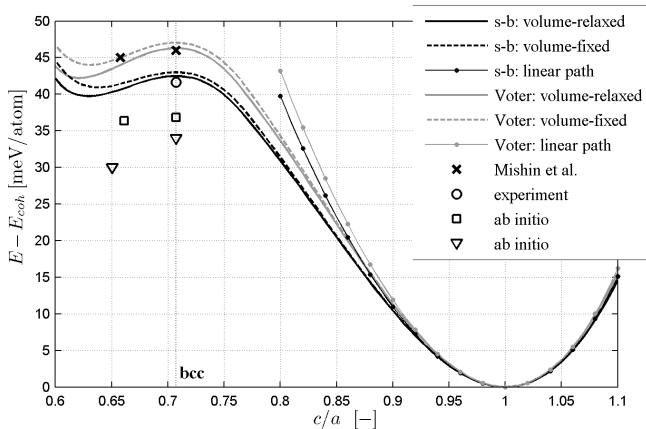

Fig. 8. Crystal energy change along three Bain paths predicted by the s-b and Voter models. For comparison, the experimental and ab initio structural energy differences $\Delta E_{fcc \to bcc}$ and $\Delta E_{fcc \to bct}$ (Table 6) are also shown

Table 6

Characterizations of the Cu metastable phases bcc, bct and sc obtained by the EAM models in comparison with the experimental and ab initio data: structural energy difference (ΔE in meV), volume per atom referred to the equilibrium value (V/V_0)) and ratio of the tetragonal cell edges (c/a)

	s-b	Voter	Exp./Ab initio	Mishin
$\Delta E_{fcc \to bcc}$	42.5	46.3	41.7[a], 36.8[b], 34.0[c]	46.0
V/V_0	1.01	1.01	1.00[c]	1.00
$\Delta E_{fcc \to bct}$	39.7	42.2	36.4[b] 30.0[c]	45.0
c/a	0.63	0.62	0.66[b] 0.65[c]	0.66
V/V_0	1.02	1.02	1.00[c]	1.00
$\Delta E_{fcc \to sc}$	417.4	417.0	446[c], 464.8[d]	433
V/V_0	1.17	1.18	1.17[c]	1.16

[a] Ref. [33], [b] Ref. [39], [c] Ref. [40], [d] Ref. [41].

In the range of small strains, the Voter model reproduces the considered Bain processes with the error $D^{\Phi}(\varepsilon_{II}) = 9.4\%$. Too fast increase in the energy results in the too high transition energy $\Delta E_{fcc \to bcc}$ in comparison with the experimental and ab initio values (see Fig. 8 and Table 6). A similar effect is observed at the transformation of the fcc structure into the body centered tetragonal (bct) one. The error in the second Kelvin modulus $D^{\Phi}(\varepsilon_{II})$ for the proposed potential is significantly lower therefore, the Bain processes are reproduced more correctly. The Mishin et al. model predicts the high values of the energy differences on account of fitting to the ab initio data.

The trigonal path is another deformation process which connects metastable phases of fcc crystals. In the present paper, this path is realized by means of a hexagonal elementary cell with the edges $a = \frac{1}{2}[1\,\overline{2}\,1]a_0$, $b = \frac{1}{2}[1\,1\,\overline{2}]a_0$ and $c = [1\,1\,1]a_0$ in the cubic system (see Fig. 9). The cell recreates the fcc lattice and additionally its orientation is observed by the HRTEM in Cu epitaxial layers formed on $(0\,0\,0\,1)\alpha - Al_2O_3$ substrates. Along the trigonal path, the cell base is uniformly extended and the height compressed. When $c/a = \sqrt{2}/2$ the simple cubic (sc) structure is formed. Subsequently for $c/a = \sqrt{2}/4$, the body centered structure arises (Fig. 9). The deformations along the trigonal path are such as in the Bain process; although they are imposed on the different cell. Therefore, both the path with the fixed volume and the linear one are described by the same strain tensors $E_B(e)$ and $E_{B.L}(e)$, but in the reference system of the hexagonal cell: $\hat{x}_H = [1-2\,1]/\sqrt{6}$, $\hat{y}_H = [1\,0-1]/\sqrt{2}$ and $\hat{z}_H = [1\,1\,1]/\sqrt{3}$. In the cubic system, the tensor $E_{B.L}$ takes the form:

$$E_{T.L}(e) = e \begin{pmatrix} 0 & -1 & -1 \\ -1 & 0 & -1 \\ -1 & -1 & 0 \end{pmatrix}. \quad (27)$$

Thus, the trigonal path begins in the third eigensubspace of the elasticity tensor. If the potential predicts the third Kelvin modulus with some inaccuracy the committed error occurs in successive stages of the trigonal process in the range of small strains. This disturbance influences energy changes at large deformations.
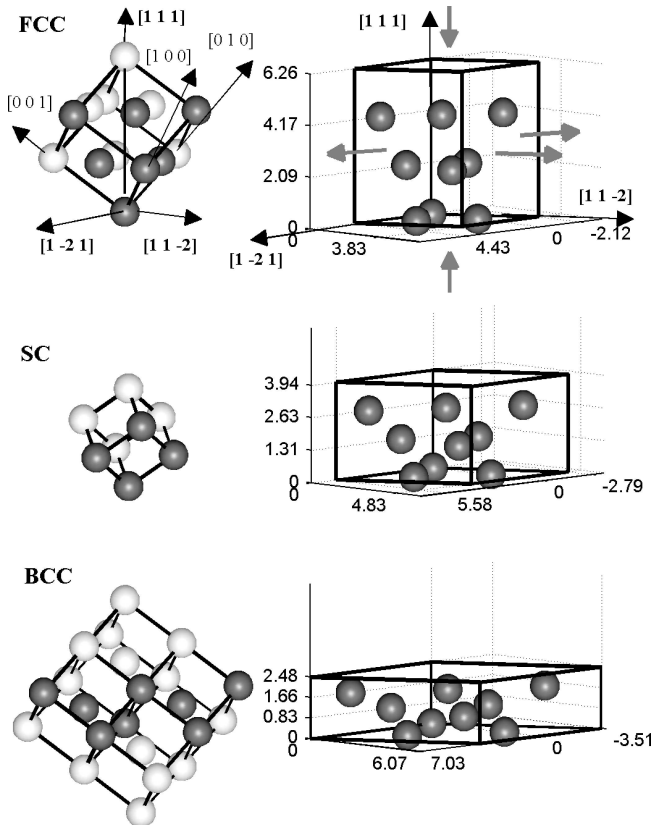
Fig. 9. Trigonal deformation of the fcc structure resulting in the simple cubic and body centered cubic structures
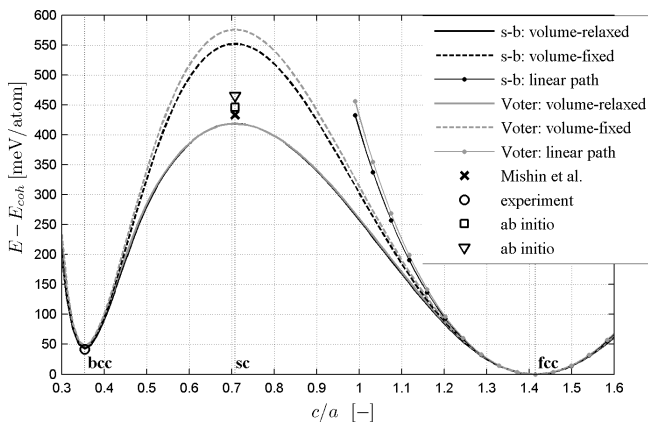

Fig. 10. Crystal energy change along three trigonal paths predicted by the s-b and Voter models. For comparison, the experimental and ab initio structural energy differences $\Delta E_{fcc \to sc}$ and $\Delta E_{fcc \to bcc}$ (Table 6) are also shown

Both the proposed model and the Voter one predict λ_{III} inaccurately. The s-b potential determines the modulus with the larger error (-2.6%). Therefore, along the trigonal path, we obtain slower increase in the crystal energy per atom than in the case of the Voter model (see Fig. 10). Despite this, the fcc-sc structural energy difference is slightly closer to the ab initio values [40, 41] than $\Delta E_{fcc \to sc}$ determined by the Voter potential (see Table 6). The final result depends not only on the path initiation but also on other factors including the volume relaxation of the sc structure. The relaxation is de-termined in large measure by repulsive interactions between a central atom and its neighbors. In the Voter model, the repulsion is larger on account of the form of the embedding energy (see Fig. 1). Therefore, during the relaxation, there is the larger increase in the volume and as a result the value of the $\Delta E_{fcc \to sc}$ is slightly lower than that predicted by the s-b potential. Summing up, the correctness of the Kelvin modulus is one of the factors which condition accurate reconstruction of the trigonal processes. Therefore, a small error in the prop-erty has little influence on the obtained characterizations of the metastable phases.

4. Conclusions

Material symmetry determines the elementary processes of deformations. The present work shows that the errors in the energy densities of these processes, that is in the Kelvin mod-uli, determine the range of inaccuracies with which a model reproduces small-strain processes. Such an estimation is possi-ble because the errors in the Kelvin moduli constitute extrema of the function which ascribes errors in energy densities to different small-strain processes. The elementary processes ini-tiate the key paths of large deformations. Therefore, the con-siderable errors in the Kelvin moduli result in incorrect repro-ducing the structural transformations: fcc-bcc, fcc-sc as well as fcc-bct. The elastic constants do not have such properties as the Kelvin moduli. As a result, despite small errors in these constants, a model can reproduce certain small-strain process-es with large inaccuracy. If the tetragonal or trigonal paths undergo disturbances the fcc-bcc or fcc-sc structural trans-formations are recreated incorrectly. Thus, the present work identifies the relation which symmetry introduces between the elastic properties of material and structural transformations. Applying the description of the atom environment in terms of neighbor spheres, the formula of the unrelaxed stacking fault energy useful for an EAM model parametrization has been obtained. The mentioned description also allows identi-fying the symmetry-based relation between the fcc structure with the stacking fault and the hcp one. As a result, the rela-tionship between the unrelaxed stacking fault energy and hcp structural energy is obtained. Summing up, material symme-try indicates key properties for a model specification. Using them, we obtain a potential which better describes processes of small and large deformations.

The conclusion presented above has been confirmed by the specification of the Voter model describing interatomic interactions in copper. For the parametrization, the set of the properties considered by Voter has been used but the Kelvin moduli have been applied instead of the elastic constants. The relationships for the specification of the model have been ex-pressed in a particularly simple way due to application of the symmetry relations. As a result, the potential which more ac-curately reproduces small strain processes and the key paths of large deformations has been obtained. Additionally, defect formation as well as Cu dimer properties are predicted in a good agreement with the experiments.

REFERENCES

[1] K. Dems and Z. Mróz, "Analysis and design of thermo-mechanical interfaces", *Bull. Pol. Ac.: Tech.* 60, 205–213 (2012).

[2] G. Szefer and D. Jasińska, "Modeling of strains and stresses of material nanostructures", *Bull. Pol. Ac.: Tech.* 57, 41–46 (2009).

[3] J. Rychlewski, "On Hooke's law", *J. Applied Mathematics and Mechanics* 48, 303–314 (1984).

[4] K. Nalepka, "Symmetry-based approach to parametrization of embedded-atom-method interatomic potentials", *Comp. Mater. Sci.* 56, 100–107 (2012).

[5] A.F. Voter, *Los Alamos Unclassified Technical Report No. LA-UR 93-3901*, 1993, unpublished.

[6] A.F. Voter, "Parallel replica method for dynamics of infrequent events", *Phys. Rev.* B 57 (R 13), 985–988 (1998).

[7] J.H. Rose, J. Ferrante, and J.R. Smith, "Universal binding energy curves for metals and bimetallic interfaces", *Phys. Rev. Lett.* 47, 675–678 (1981).

[8] A. Banerjea and J.R. Smith, "Origins of the universal binding-energy relation", *Phys. Rev.* B 37, 6632–6645 (1988).

[9] F.H. Streitz and J.W. Mintmire, "Electrostatic potentials for metal-oxide surfaces and interfaces", *Phys. Rev.* B 50, 11996–12003 (1994).

[10] K. Nalepka, "Efficient approach to metal/metal oxide interfaces within variable charge model", *Eur. Phys. J.* B 85, 45 (2012).

[11] M.S. Daw and M.I. Baskes, "Embedded atom metod: derivation and application to impurities, surfaces, and other defects in metals", *Phys. Rev.* B 29, 6443–6453 (1984).

[12] K. Nalepka and R.B. Pęcherski, "Modeling of the interatomic interactions in the copper crystal applied in the structure $(111)Cu||(0001)Al_2O_3$", *Archives of Metallurgy and Materials* 54, 511–522 (2009).

[13] K. Kowalczyk-Gajewska and J. Ostrowska-Maciejewska, "Review on spectral decomposition of Hooke's tensor for all symmetry groups of linear elastic material", *Engng. Trans.* 57, 145–183 (2009).

[14] S. Crampin, K. Hampel, J.M. MacLaren, and D.D. Vvedensky, "The calculation of stacking fault energies in close-packed metals", *J. Mater. Res.* 5, 2107–2119 (1990).

[15] A.F. Wright, M.S. Daw, and C.Y. Fong, "Theoretical investigation of (111) stacking faults in aluminium", *Phil. Mag.* A 66, 387–404 (1992).

[16] N.M. Rosengaard and H.L. Skriver, "Calculated stacking-fault energies of elemental metals", *Phys. Rev.* B 47, 12865–12873 (1993).

[17] R. Eason, *Pulsed Laser Deposition of Thin Films: Applications-Led Growth of Functional Materials*, John Willey & Sons, Inc., New Jersey, 2007.

[18] E.A. Rohlfing and J.J. Valentini, "UV laser excited fluorescence spectroscopy of the jet-cooled copper dimer", *J. Chem. Phys.* 84, 6560–6566 (1986).

[19] K.P. Huber and G. Hertzberg, *Constants of Diatomic Molecules*, Van Nostrand Reinhold, New York, 1979.

[20] T.F. Coleman and Y. Li, "An interior, trust region approach for nonlinear minimization subject to bounds", *SIAM J. Optim.* 6, 418–445 (1996).

[21] *MATLAB Reference Guide*, The Math Works, Natick, 2011.

[22] D.R. Lide, *CRC Handbook of Chemistry and Physics*, CRC Press, Boca Raton, 1998.

[23] C.J. Smith, *Metal Reference Book*, Butterworth, London, 1976.

[24] F.R. Kroeger and C.A. Swenson, "Absolute linear thermal-expansion measurements on copper and aluminum from 5 to 320 K", *J. Appl. Phys.* 48, 853–864 (1977).

[25] P. Villars, *Pearson's Handbook Desk Edition: Crystallographic Data for Intermetallic Phases*, ASM International, Materials Park, 1997.

[26] W.C. Overton JR. and J. Gaffney, "Temperature variation of the elastic constants of cubic elements. I. Copper", *Phys. Rev.* B 98, 969–977 (1955).

[27] Y.A. Chang and L. Himmel, "Temperature dependence of the elastic constants of Cu, Ag, and Au above room temperature", *J. Appl. Phys.* 37, 3567–3572 (1966).

[28] Y. Mishin, M.J. Mehl, D.A. Papaconstantopoulos, A.F. Voter, and J.D. Kress, "Structural stability and lattice defects in copper: Ab initio, tight-binding, and embedded-atom calculations", *Phys. Rev.* B 63, 224106 (2001).

[29] W.R. Tyson and W.A. Miller, "Surface free energies of solid metals: Estimation from liquid surface tension measurements", *Surf. Sci.* 62, 267–276 (1977).

[30] D.J.H. Cockayne, M.L. Jenkins, and I.L.F. Ray, "The measurement of stacking-fault energies of pure face-centred cubic metals", *Phil. Mag.* 24, 1383–1392 (1971).

[31] P.R. Thornton and T.E. Mitchell, "Deformation twinning in alloys at low temperatures", *Phil. Mag.* 7, 361–375 (1962).

[32] L.E. Murr, *Interfacial Phenomena in Metals and Alloys*, Addison-Wesley, Reading, 1975.

[33] Y. Wang, S. Curtarolo, C. Jiang, R. Arroyave, T. Wang, G. Ceder, L.-Q. Chen, and Z.-K. Liu, "Ab initio lattice stability in comparison with CALPHAD lattice stability", *Computer Coupling of Phase Diagrams and Thermochemistry* 28, 79–90 (2004).

[34] Th. Hehenkamp, W. Berger, J.-E. Kluin, Ch. Ludecke, and J. Wolff, "Equilibrium vacancy concentrations in copper investigated with the absolute technique", *Phys. Rev.* B 45, 1998–2003 (1992).

[35] R.W. Balluffi, "Vacancy defect mobilities and binding energies obtained from annealing studies", *J. Nucl. Mater.* 69&70, 240–263 (1978).

[36] W. Lühr-Tanck, A. Sager, and H. Bosse, "The effect of vacancies and precipitation in CuIn alloys on positron annihilation", *J. Phys. F: Met. Phys.* 17, 827–836 (1987).

[37] H.J. Wollenberger, "Point Defects" in *Physical Metallurgy*, eds. R.W. Cahn and P. Haasen, Elsevier, Amsterdam, 1996.

[38] G. Grimvall, B. Magyari-Köpe, V. Ozolinš, and K.A. Persson, "Lattice instabilities in metallic elements", *Rev. Mod. Phys.* 84, 945–986 (2012).

[39] M.J. Mehl, A. Aguayo, and L.L. Boyer, "Absence of metastable states in strained monatomic cubic crystals", *Phys. Rev.* B 70, 014105 (2004).

[40] M. Černý, R. Boyer, M. Šob, and S. Yip, "Higher-energy structures and stability of Cu and Al crystals along displacive transformation paths", *J. Computer-Aided Materials Design* 12, 161–173 (2005).

[41] X.D. Dai, Y. Kong, and J.H. Li, "Long-range empirical potential model: Application to fcc transition metals and alloys", *Phys. Rev.* B 75, 104101 (2007).